Bollettino
Unione Matematica Italiana

Marco Prato

A Deconvolution Algorithm for Imaging Problems from Fourier Data

Bollettino dell'Unione Matematica Italiana, Serie 9, Vol. **6** (2013), n.2, p. 389–404.

Unione Matematica Italiana

<http://www.bdim.eu/item?id=BUMI_2013_9_6_2_389_0>

L'utilizzo e la stampa di questo documento digitale è consentito liberamente per motivi di ricerca e studio. Non è consentito l'utilizzo dello stesso per motivi commerciali. Tutte le copie di questo documento devono riportare questo avvertimento.

Articolo digitalizzato nel quadro del programma
bdim (Biblioteca Digitale Italiana di Matematica)
SIMAI & UMI
http://www.bdim.eu/

Bollettino dell'Unione Matematica Italiana, Unione Matematica Italiana, 2013.

Bollettino U. M. I.
(9) **VI** (2013), 389-404

A Deconvolution Algorithm for Imaging Problems from Fourier Data

MARCO PRATO

Abstract. – *In this paper we address the problem of reconstructing a two-dimensional image starting from the knowledge on nonuniform samples of its Fourier Transform. Such inverse problem has a natural semidiscrete formulation, that is analyzed together with its fully discrete counterpart. In particular, the image restoration problem in this case can be reformulated as the minimization of the data discrepancy under nonnegativity constraints, possibly with the addition of a further equality constraint on the total flux of the image. Moreover, we show that such problem is equivalent to a deconvolution in the image space, that represents a key property allowing the desing of a computationally efficient algorithm based on Fast Fourier Transforms to address its solution. Our proposal to compute a regularized solution in the discrete case involves a gradient projection method, with an adaptive choice for the steplength parameter that improves the convergence rate. A numerical experimentation on simulated data from the NASA RHESSI mission is also performed.*

1. – Introduction

In many imaging problems, one has to reconstruct a two-dimensional image of a certain object starting from the knowledge of one or more corrupted versions of it, depending in general of the data acquisition system that introduces blurring effects and statistical noise. In this cases, the data and the unknown are both "vectorized" images, possibly with different size, whose relation can often be assumed as linear thanks to the use of suitable physical approximations. In imaging problems arising in several scientific areas (e.g., radioastronomy, X-ray astronomy, computed tomography, magnetic resonance imaging [7, 13, 21]), instead, the data belong to a space different from the one of the unknown object. In particular, the specific nature of the acquisition system provides measures (or estimates) of the Fourier Transform of the object in a set of hardware-depending spatial frequencies. In the general case, the distribution of such frequencies in the Fourier plane is highly sparse and irregular, with specific zones in which the data are concentrated side by side to other areas with a total lack of information. This problem presents both theoretical and computational difficulties: from the theoretical point of view, we are dealing with an inverse problem which is ill

posed in the sense of Hadamard [22]. In fact, due to the sparsity of the samples in the frequency space, infinite solutions are admissible; moreover, some of these solutions could not be physically meaningful because of the error which potentially affects the data. On the other hand, from the computational point of view, the possible strong irregularity of the data sampling makes the use of the Nonuniform Fast Fourier Transform (NFFT) algorithm [17] very dangerous, since the choice of the interpolation strategy at the basis of NFFT could play a crucial role in arbitrarily filling the areas in the frequency space which lack in information. Moreover, for measured data affected by a high level of noise, the interpolation phase may lead to an amplification of this noise level on the resampled data with the result of artifacts formation and undesirable effects in the corresponding reconstructed image.

Here we propose an alternative strategy to reconstruct the desired image from the available set of Fourier samples that does not perform any interpolation and resampling procedure, thus avoiding arbitrary assumptions and possible noise amplifications. In particular, we reformulate the imaging problem as a constrained optimization problem, in which the stationary points of the objective function can be viewed as the solutions of a deconvolution problem with a suitable kernel. We propose a fast and effective gradient projection algorithm to provide regularized solutions of such a deconvolution problem by early stopping the iterations [2, 11]. An adaptive steplength parameter choice is adopted to improve the converge rate of the algorithm; more in details, we implemented a suitable alternation of the two Barzilai-Borwein rules [1], which recently obtained very good results in signal and image denoising and deblurring problems [2, 11, 28, 32]. Since the objective function involves a convolution operator, the algorithm can be effectively implemented exploiting the (uniform) Fast Fourier Transform.

The paper is divided in five further sections. In particular, sections 2 and 3 are devoted to the semidiscrete and fully discrete mathematical formulation of the problem, respectively. The analytic expression of its generalized solution is provided and the equivalent constrained optimization problem is deduced through the introduction of a particular convolution operator. In section 4, the optimization algorithm is described and the regularization issue is discussed. Numerical experiments involving synthetic data from a real-world astronomical application are given in section 5, while some conclusions and ideas for future developments of the method are offered in section 6.

2. – From Fourier samples to the continuous object

Inverse problems in which continuous functions have to be inferred from the knowledge of a measurements array are called semidiscrete problems [3, 4]. In

our case, the unknown is a non-negative two-dimensional distribution $f(x,y)$ defined on a square $\mathcal{I}=[X_1,X_2]\times[Y_1,Y_2]$ in the image plane, while the data array $g\in\mathbb{C}^M$ consists in a certain number of the object's Fourier Transform estimates corresponding to the spatial frequencies (u_k,v_k), $k=1,\dots,M$, according to the relation

$$g_k=\int_{\mathcal{I}} f(x,y)e^{2\pi i(u_kx+v_ky)}dxdy. \tag{1}$$

Each component k of the data array can be considered as the evaluation of a continuous distribution

$$V(u,v)=\int_{\mathcal{I}} f(x,y)e^{2\pi i(ux+vy)}dxdy,\quad (u,v)\in\mathbb{R}^2 \tag{2}$$

in the specific frequencies (u_k,v_k). We consider the Hilbert space $X=L^2(\mathcal{I},\mathbb{C})$ and the semidiscrete operator $\mathcal{H}:X\to\mathbb{C}^M$ defined as

$$(\mathcal{H}f)_k=\int_{\mathcal{I}} f(x,y)e^{2\pi i(u_kx+v_ky)}dxdy,\quad k=1,\dots,M,\quad f\in X. \tag{3}$$

The adjoint of the operator $\mathcal{H}$, $\mathcal{H}^*:\mathbb{C}^M\to X$, also called back-projection, is defined as follows: given $c\in\mathbb{C}^M$

$$(\mathcal{H}^*c)(x,y)=\sum_{k=1}^{M} c_ke^{-2\pi i(u_kx+v_ky)},\quad (x,y)\in\mathcal{I}. \tag{4}$$

Indeed, we have

$$\begin{aligned}\langle\mathcal{H}f,c\rangle_{\mathbb{C}^M}&=\sum_{k=1}^{M}c_k\int_{\mathcal{I}}\overline{f(x,y)}e^{-2\pi i(u_kx+v_ky)}dxdy\\&=\int_{\mathcal{I}}\overline{f(x,y)}\sum_{k=1}^{M}c_ke^{-2\pi i(u_kx+v_ky)}dxdy=\langle f,\mathcal{H}^*c\rangle_X\end{aligned}$$

where $\langle\cdot,\cdot\rangle_{\mathbb{C}^M}$ and $\langle\cdot,\cdot\rangle_X$ denote the inner product of $\mathbb{C}^M$ and X, respectively.

Thus, the image reconstruction problem can be formulated as a linear inverse problem with discrete data [4]

$$\mathcal{H}f=g, \tag{5}$$

which is ill posed since it has infinite solutions.

We show now that equation (5) is equivalent to a deconvolution problem in the space domain. If we recall definition (2), we observe that the discrete data g_k can

be expressed as

$$g_k = V(u_k, v_k) = \int_{\mathbb{R}^2} \delta(u - u_k, v - v_k) V(u, v) du dv, \quad k = 1, \dots, M.$$

By introducing the sampling function $S(u, v) = \sum_{k=1}^{M} \delta(u - u_k, v - v_k)$, we define the "dirty image" f_d as the Fourier Transform of the product SV:

$$f_d \underset{\mathcal{F}}{\overset{\mathcal{F}^{-1}}{\rightleftarrows}} SV.$$

In particular, for $(x, y) \in \mathcal{I}$, we have

$$\begin{aligned} f_d(x, y) &= \int_{\mathbb{R}^2} S(u, v) V(u, v) e^{-2\pi i(ux+vy)} du dv \\ &= \sum_{k=1}^{M} \int_{\mathbb{R}^2} \delta(u - u_k, v - v_k) V(u, v) e^{-2\pi i(ux+vy)} du dv \\ &= \sum_{k=1}^{M} g_k e^{-2\pi i(u_k x + v_k y)} = (\mathcal{H}^* g)(x, y). \end{aligned} \tag{6}$$

Using the Convolution Theorem, the function f_d can be expressed as the convolution of the inverse Fourier Transform of S and V (see figure 1):

$$K * f \underset{\mathcal{F}}{\overset{\mathcal{F}^{-1}}{\rightleftarrows}} SV,$$

where K is the Fourier Transform of the sampling function S

$$K \underset{\mathcal{F}}{\overset{\mathcal{F}^{-1}}{\rightleftarrows}} S$$

SPACE		FREQUENCY
f	$\overset{\mathcal{F}^{-1}}{\rightarrow}$	V
Convolution $\downarrow$		$\downarrow$ *Sampling*
f_d	$\underset{\mathcal{F}}{\leftarrow}$	SV

Fig. 1. – Space-frequency scheme.

defined, for $(x,y) \in \mathbb{R}^2$, as

$$
\begin{aligned}
K(x,y) &= \int_{\mathbb{R}^2} S(u,v) e^{-2\pi i(ux+vy)} du dv \\
&= \sum_{k=1}^{M} \int_{\mathbb{R}^2} \delta(u-u_k, v-v_k) e^{-2\pi i(ux+vy)} du dv \\
&= \sum_{k=1}^{M} e^{-2\pi i(u_k x + v_k y)}.
\end{aligned} \tag{7}
$$

Thus, the image reconstruction problem can be formulated also as a deconvolution problem in the space domain: find a function $f \in L^2(\mathcal{I})$ such that

$$K * f = f_d. \tag{8}$$

We remark that, for $f \in X$ and $(x,y) \in \mathcal{I}$,

$$
\begin{aligned}
(K*f)(x,y) &= \int_{\mathcal{I}} K(x-x', y-y') f(x',y') dx' dy' \\
&= \int_{\mathcal{I}} \left(\sum_{k=1}^{M} e^{-2\pi i(u_k(x-x')+v_k(y-y'))} \right) f(x',y') dx' dy' \\
&= \sum_{k=1}^{M} e^{-2\pi i(u_k x + v_k y)} \left(\int_{\mathcal{I}} f(x',y') e^{2\pi i(u_k x' + v_k y')} dx' dy' \right) \\
&= \sum_{k=1}^{M} (\mathcal{H}f)_k e^{-2\pi i(u_k x + v_k y)} = (\mathcal{H}^* \mathcal{H} f)(x,y)
\end{aligned}
$$

and, therefore, that

$$\|K * f - f_d\|_X^2 = \|\mathcal{H}^* \mathcal{H} f - \mathcal{H}^* g\|_X^2. \tag{9}$$

From the identity

$$\|\mathcal{H}^* \mathcal{H} f - \mathcal{H}^* g\|_X^2 = (\mathcal{H}f - g)^* \mathcal{H} \mathcal{H}^* (\mathcal{H}f - g) = \|\mathcal{H}f - g\|_{\mathbb{C}^M, \mathcal{H}\mathcal{H}^*}^2, \tag{10}$$

we can see that the data discrepancy measured in the norm in $\mathbb{C}^M$ induced by the Gram matrix $\mathcal{H}\mathcal{H}^*$ can be expressed by means of a convolution in the space X.

Since it is natural in an image reconstruction problem to require the radiation flux to be real and non-negative, we are interested in solving the minimization problem

$$\min_{\substack{f \in L^2(\mathcal{I}, \mathbb{R}) \\ f \geq 0}} J(f), \tag{11}$$

where $J(f)$ is one of the equivalent distance measures defined in (9) or (10). Moreover, it could be useful to insert also an equality constraint

$$\int_{\mathcal{I}} f(x,y)dxdy = F,$$

where F represents the total flux emitted by the source and inferred in some way from the data. We observe that problem (11) can be still ill-posed, since the set of nonnegative functions is closed and convex in L^2 but not compact.

3. – Discrete formulation

Although in principle the semidiscrete problem can be solved with classical approaches with a resulting continuous solution for the unknown discribution, in practice a discrete version of the problem described in section 2 is considered, thus leading to a target object in the form of a matrix. To this aim, we consider a uniform grid over the square $\mathcal{I}$ given by the points

$$x_j = X_1 + (j-1)\Delta x,\ \ y_h = Y_1 + (h-1)\Delta y, \quad j,h = 1,...,N$$

and we discretize the integral of equation (1) by the rectangular rule obtaining a vector $g \in \mathbb{C}^M$ with

$$g_k \approx \sum_{j,h=1}^{N} f(x_j,y_h)e^{2\pi i(u_k x_j + v_k y_h)}\Delta x \Delta y, \quad k = 1,...,M.$$

In the discrete settings, we would like to find an approximation of the values

$$f_{jh} = f(x_j,y_h)\Delta x \Delta y, \quad j,h = 1,...,N.$$

Therefore, given a vector $f_{jh} \in \mathbb{C}^{N^2}$, we define the linear operator H as

$$(Hf)_k = \sum_{j,h=1}^{N} f_{jh}e^{2\pi i(u_k x_j + v_k y_h)}, \quad k = 1,...,M \tag{12}$$

and its adjoint is

$$(H^* c)_{jh} = \sum_{k=1}^{M} c_k e^{-2\pi i(u_k x_j + v_k y_h)}, \quad j,h = 1,...,N, \tag{13}$$

where $c \in \mathbb{C}^M$. The operators (12) and (13) can be considered a numerical approximation of (3) and (4); in these settings, the discrete inverse problems is given by

$$Hf = g.$$

Following the process described in section 2, now we discuss the discrete version of equation (8). With the same settings introduced before, we define the grid points

$$x_j = X_1 + (j-1)\Delta x,\ \ y_h = Y_1 + (h-1)\Delta y, \quad j,h = -N, -(N-1), ..., 0$$

and denote by K_{jh} the values $K(x_j, y_h)\Delta x \Delta y$ $(j,h = -N, \dots, N)$.

Thus, the discrete counterpart of (8) becomes

$$\begin{aligned}
(K * f)(x_p, y_q) &= \sum_{jh=1}^{N} f_{jh} K_{p-j,q-h} \\
&= \sum_{jh=1}^{N} f_{jh} \sum_{k=1}^{M} e^{-2\pi i(u_k(x_p - x_j) + v_k(y_q - y_h))} \\
&= \sum_{k=1}^{M} e^{-2\pi i(u_k x_p + v_k y_q)} \sum_{jh=1}^{N} f_{jh} e^{2\pi i(u_k x_j + v_k y_h)} \\
&= \sum_{k=1}^{M} e^{-2\pi i(u_k x_p + v_k y_q)} (Hf)_k \\
&= (H^* H f)_{pq},
\end{aligned} \tag{14}$$

where (x_p, y_q) is a grid point and H, H^* are defined in (12) and (13), respectively.

Since

$$f_d(x_j, y_h) = \sum_{k=1}^{M} g_k e^{-2\pi i(u_k x_j + v_k y_h)} = (H^* g)_{jh}, \quad j,h = 1, ..., N, \tag{15}$$

we can write the analogous result in (9) as

$$\|K * f - f_d\|^2_{\mathbb{C}^{N^2}} = \|H^* H f - H^* g\|^2_{\mathbb{C}^{N^2}}. \tag{16}$$

We remark that also in the fully discrete setting we can write the identity

$$\|H^* H f - H^* g\|^2_{\mathbb{C}^{N^2}} = (Hf - g)^* H H^* (Hf - g) = \|Hf - g\|^2_{\mathbb{C}^M, HH^*}, \tag{17}$$

which shows the equivalence between the deconvolution problem and the least squares one in the norm induced by the Gram matrix.

Therefore, our optimal real positive radiation flux image will be the solution of the following minimum problem in the space domain:

$$\begin{aligned}
&\min && J(f), \\
&f \in \mathbb{R}^{N^2} && \\
&f \geq 0 &&
\end{aligned} \tag{18}$$

where $J(f)$ is one of the equivalent distance measures defined in (16) or (17).

As in the semi-discrete case, the flux conservation condition can be easily imposed by adding the equality

$$\sum_{jh=1}^{N} f_{jh} = F$$

to the constraints of problem (18), where again F represents the total flux emitted by the source.

4. – The Space-D algorithm

The simple form of the constraint to be imposed on the unknown image suggested us to adopt a gradient projection (GP) method [5, 6, 11, 30] to address the numerical solution of (18). The GP approach can be applied to any minimization problem

$$\min_{f \in \mathcal{C}} \quad J(f) \tag{19}$$

where J is a differentiable real valued function and $\mathcal{C}$ is a convex closed subset of $\mathbb{R}^m$. Clearly, problem (18) is a special case of (19), since, even if the data are complex numbers, the objective function is real valued and its variable is constrained in a subset of $\mathbb{R}^{N^2}$. The general form of the GP algorithm is described in Algorithm 1, where $\mathcal{P}_{\mathcal{C}}$ denotes the orthogonal projection on the set $\mathcal{C}$.

Algorithm 1 Gradient Projection (GP) Method

Choose the starting point $f^{(0)} \in \mathcal{C}$, set the parameters $\beta, \theta \in (0,1)$, $0 < \alpha_{min} < \alpha_{max}$ and fix a positive integer K.

FOR $k = 0, 1, 2, \ldots$ DO THE FOLLOWING STEPS:

STEP 1. Choose the parameter $\alpha_k \in [\alpha_{min}, \alpha_{max}]$;

STEP 2. Projection: $y^{(k)} = P_{\mathcal{C}}(f^{(k)} - \alpha_k \nabla J(f^{(k)}))$;

STEP 3. Descent direction: $d^{(k)} = y^{(k)} - f^{(k)}$;

STEP 4. Set $\lambda_k = 1$ and $J_{max} = \max_{0 \le j \le \min(k, K-1)} J(f^{(k-j)})$;

STEP 5. Backtracking loop:

let $J_{new} = J(f^{(k)} + \lambda_k d^{(k)})$;

IF $J_{new} \le J_{max} + \beta \lambda_k \nabla J(f^{(k)})^T d^{(k)}$ THEN

go to Step 6;

ELSE

set $\lambda_k = \theta \lambda_k$ and go to Step 5.

ENDIF

STEP 6. Set $f^{(k+1)} = f^{(k)} + \lambda_k d^{(k)}$.

END

In practice, each SGP iteration is based on the descent direction $d^{(k)}$, obtained as the difference between the current point $f^{(k)}$ and the projection $y^{(k)}$ of the scaled gradient on the feasible set. The global convergence of the algorithm is obtained by means of the standard monotone Armijo rule in the linesearch procedure described in step 5 (see [11]). We emphasize that any choice of the steplength $\alpha_k \in [\alpha_{min}, \alpha_{max}]$ is allowed; this freedom of choice can then be fruitfully exploited for introducing performance improvements. An effective selection strategy is obtained by means of the Barzilai and Borwein [1] rules (hereafter denoted BB), defined as

$$\alpha_k^{(1)} = \frac{{s^{(k-1)}}^T s^{(k-1)}}{{s^{(k-1)}}^T t^{(k-1)}} \quad ; \quad \alpha_k^{(2)} = \frac{{s^{(k-1)}}^T t^{(k-1)}}{{t^{(k-1)}}^T t^{(k-1)}}, \tag{20}$$

where $s^{(k-1)} = f^{(k)} - f^{(k-1)}$ and $t^{(k-1)} = \nabla J(f^{(k)}) - \nabla J(f^{(k-1)})$. In our GP implementation, the values produced by these rules are constrained into the interval $[\alpha_{min}, \alpha_{max}]$ in the following way:

IF $(s^{(k-1)})^T t^{(k-1)} \leq 0$ THEN
  $\alpha_k^{(1)} = \min\{10 \cdot \alpha_{k-1},\ \alpha_{max}\}$;
ELSE
  $\alpha_k^{(1)} = \min\left\{\alpha_{max},\ \max\left\{\alpha_{min},\ \alpha_k^{(BB1)}\right\}\right\}$;
ENDIF
IF $(s^{(k-1)})^T t^{(k-1)} \leq 0$ THEN
  $\alpha_k^{(2)} = \min\{10 \cdot \alpha_{k-1},\ \alpha_{max}\}$;
ELSE
  $\alpha_k^{(2)} = \min\left\{\alpha_{max},\ \max\left\{\alpha_{min},\ \alpha_k^{(BB2)}\right\}\right\}$;
ENDIF

The recent literature on steplength selection in gradient methods showed that remarkable convergence rate improvements can be obtained by alternation strategies of the two BB formulae [30, 33] that force the selection to be made in a suitable order of both low and high BB values. Frassoldati et al. [20] realized this aim by means of an alternation criterion, which compares well with other popular BB-like steplength rules, namely

IF $\alpha_k^{(2)} / \alpha_k^{(1)} \leq \tau_k$ THEN
  $\alpha_k = \min_{j=\max\{1,k+1-M_\alpha\},\ldots,k} \alpha_j^{(2)}$;
  $\tau_{k+1} = 0.9 \cdot \tau_k$;
ELSE
  $\alpha_k = \alpha_k^{(1)}$;
  $\tau_{k+1} = 1.1 \cdot \tau_k$;
ENDIF

where M_α is a prefixed positive integer and $\tau_1 \in (0,1)$. As observed in several experimental studies [2, 11], the GP method equipped with this alternation of the two BB formulas is more efficient with respect to the same algorithm with other steplength selection rules and also to other iterative approaches as the projected Landweber method [18].

About the complexity of the algorithm, the main tasks are the computation of the objective function $J(f)$ at every backtracking loop and the gradient $\nabla J(f)$ at each main iteration, both depending of the quantities $H^*Hf^{(k)}$ and H^*g. We remark that H^*g, that is the dirty image f_d, needs to be computed only once at the beginning by formula (15), while, thanks to the equivalence (14), the matrix–vector product H^*Hf can be efficiently computed by the FFT algorithm. Thus, taking into account of the zero boundary conditions on the reconstructed image, the cost per iteration is $\mathcal{O}(2n^2 \log(2n^2))$.

The last (but not the least) aspect we have to take into account is the criterion adopted to arrest the iterations. Since problem (18) is ill conditioned and the data are affected by noise, some regularization techniques are needed to achieve a meaningful solution. Even if a rigorous theoretical study is not yet available, the numerical experience on image reconstruction from noisy data demonstrates that the GP method exhibits the semiconvergence property [3, 19]: the results of the iterations first provide better and better approximations of the true object but after a certain point they turn to the worse, due to increased noise propagation. Therefore, regularization is obtained in practice by a suitable stopping of the iterations: in this way, the GP algorithm is employed as an iterative regularization method. We chose a stopping rule based on Morozov's discrepancy equation [19, 31]. In particular, we assume that the measured data g^δ can be represented in the form $g^\delta = g + \delta g$, where δg denotes the noise affecting and $g = Hf$, where f is the object to be reconstructed. Furthermore, we assume that the quantity $\eta = \|\delta g\|$ (or an estimate of it, as in the case of the application described in the following section) is known. Then, a regularized solution $f^{(k)}$ is computed if we terminate the optimization procedure when

$$\|Hf^{(k)} - g^\delta\| \leq \eta \tag{21}$$

As far as we know, no result exists proving that this criterion, applied to the GP iteration, leads to a regularization method for the constrained least square problem (18). However, in [2] it has been shown the practical effectiveness of the GP method equipped with criterion (21) on image deconvolution problems.

Moreover, we include a further stopping condition based on the relative difference of the objective function between two successive iterates

$$|J(f^{(k)}) - J(f^{(k-1)})| < \varepsilon |J(f^{(k)})| \tag{22}$$

where ε is a prefixed tolerance (in the following numerical tests we used $\varepsilon = 10^{-4}$). The criterion (22) is a quite standard condition to check the con-

vergence of an iterative optimization algorithm. Its main purpose is to devise the point where no significative decrease in the objective function is obtained (see for example [32]). We include this condition in our algorithm since, from the numerical experience, the discrepancy criterion alone may terminate the optimization procedure too soon [2], especially when the error norm η is overestimated.

In summary, our proposal is a gradient projection method with a suitable alternation of the two BB rules for the steplength selection and a combination of Morozov's discrepancy principle with the further stopping rule (22) to arrest the iterations. The resulting algorithm will be referred with the name *Space-D*.

5. – Numerical experiments: the RHESSI mission

In this section we show some numerical experiments to test the efficacy of Space-D in a real-world context. The particular application we consider is the reconstruction of the X-ray emission during solar flares starting from the data collected by the Reuven Ramaty High Energy Solar Spectroscopic Imager (RHESSI), launched from Cape Canaveral on February 5 2002 with the aim to recover temporally, spatially and spectrally resolved X-ray and γ-ray images of solar eruptions [24, 25]. The RHESSI satellite is still working and keeps on providing every day a large amount of data with very high quality.

The RHESSI instruments design is based on the Rotating Modulation Collimator (RMC) technique [23], that is a widely used approach for X-ray imaging that does not require focusing optics. Thanks to its nine bigrid RMC system, imaging information is recorded as a set of complex numbers, called *visibilities* (varying from tens to two or three hundreds according to the strength of the signal), measured at spatial frequencies arranged around nine concentric circles in the Fourier plane whose radii form a geometric sequence with common ratio $\sqrt{3}$. An example of a typical sampling of RHESSI data in the Fourier plane is shown in figure 2, where we can see that, especially in the high frequencies where the sampling is more sparse, the impact of the interpolation method can be non negligible.

The tests we present in this paper are divided in two groups. First, we simulate images with different geometries and we show the Space-D capability of providing satisfactory reconstructions independently of the object's shape. Afterwards, we investigate the very challenging task of detecting a faint source in presence of a stronger one, that represents a sort of measure of the resolution achievable by a method. Further tests on simulated and real data can be found in [9, 10]. All the simulations have been created by means of the *hsi_modelcbe2image.pro* routine, written in Interactive Data Language (IDL) and available within the official Solar SoftWare (SSW) of the RHESSI mission. For all the simulations, a comparison of the Space-D results with the ones achieved with a Maximum Entropy Method

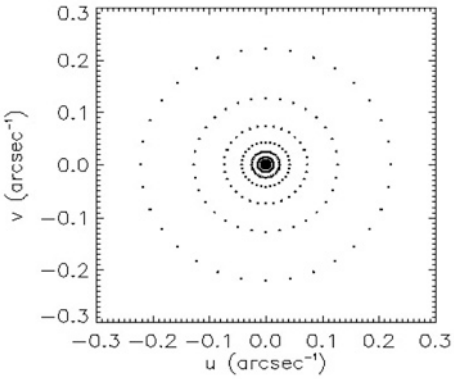

Fig. 2. – Example of a typical sampling of RHESSI data in the frequency plane.

(MEM) developed for RHESSI imaging [12] has been performed. MEM is based on the maximization of an entropy functional with constraints on the chi-square and the total flux of the image. A gridding initial step is performed on the measured visibilities in order to make possible the use of the FFT algorithm in the iterative optimization procedure adopted to solve the maximization problem. The analyses have been carried out on a computer equipped with a 1.60 GHz Intel Core i7 in a Windows 7 environment.

In figure 3 we can see the reconstructions obtained by MEM and Space-D of three maps containing very different source morphologies:

- an extremely elongated source with height very close to the best spatial resolution achievable by the RHESSI hardware (SIM1);
- a sequence of four circular sources plus a weaker one placed at the left side of the other ones (SIM2);
- a compact asymmetric source surrounded by a weaker halo (SIM3).

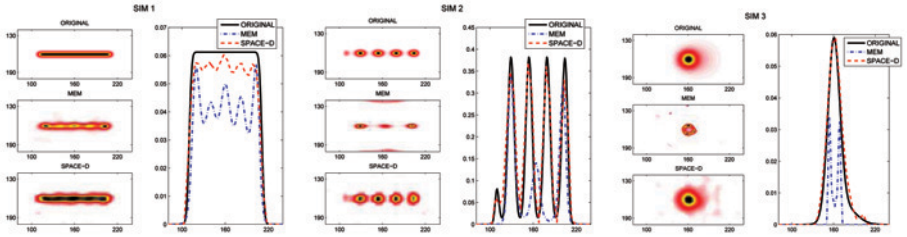

Fig. 3. — Reconstructions of the three simulations SIM1 (left panels), SIM2 (middle panels) and SIM3 (right panels) with MEM and Space-D. For each case, the restored maps and the plots of the central rows have been provided.

Due to the simulation routine, only a qualitative analysis of the reconstructions is possible, since the true pixel values are unknown. Therefore, we normalized the reconstructions so that their maximum values become equal to the reference image's one. Besides the resulting images, for a better comparison we also plotted the central rows of the true images and the corresponding reconstructions. From figure 3 we can appreciate the ability of Space-D in recovering all the different morphologies, together with the well-known tendency of MEM to overfit the data, as remarked also in [16, 26]: diffuse objects are reconstructed as a combination of sharper and narrower sources. We point out the good reconstruction of the fainter source in SIM2, that is a tough task that we further investigated with a second set of simulations.

We consider six images of two compact circular sources with equal size but different peak values, with relative ratios ranging from 1 (equal sources) to 1/30. The intermediate peaks ratios are 1/5, 1/10, 1/15 and 1/20. In figure 4 we report the same graphs provided in the previous case, namely the reconstructed maps together with the plots of the central rows. From these last curves, rather than from the images whose scale do not allow a deep investigation, we can see that Space-D recognizes the presence of a second source even in the more difficult case, while MEM behaves well only up to a peak ratio of 1/10. Such tests demonstrate the ability of Space-D in reconstructing details of the image, that are (possibly) hidden by the smooth interpolation step performed by MEM in the gridding procedure.

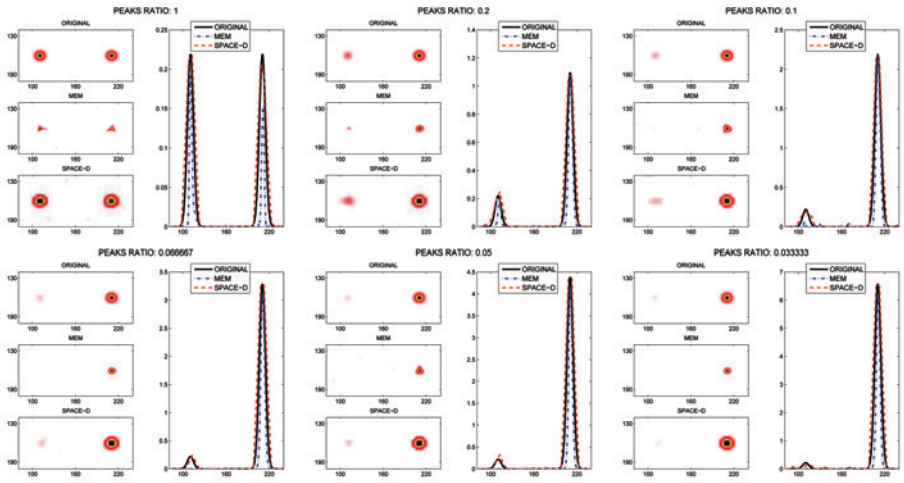

Fig. 4. – Reconstructions of the "resolution tests" with MEM and Space-D. From left to right, peaks ratios equal to 1, 1/5, 1/10, 1/15, 1/20 and 1/30 have been considered. For each case, the restored maps and the plots of the central rows have been provided.

6. – Conclusions and future work

In this paper we considered the image reconstruction problem in which the data at one's disposal are estimates or measurements of the unknown target Fourier Transform sampled nonuniformly in the frequency plane. Despite the more common approaches, we avoided to exploit interpolation techniques to resample the data on a uniform grid, since possible arbitrary impositions could be introduced in the data. Our proposal is to look for the image whose Fourier Transform is as close as possible to the measured data (in a least squares sense), with the addition of a non-negative constraint on the pixels content, that is a natural requirement for many real-world problems. The resulting formulation is a constrained optimization problem, and we addressed its solution by means of a suitable gradient method. Finally, regularization is achieved by means of an early stopping of the iterations, obtained through a combination of the Morozov's discrepancy principle with a numerical check on the objective function decrease. Simulated tests on solar X-ray images from RHESSI visibilities showed that our algorithm is able to provide effective reconstructions with different target morphologies, with a notable capability of detecting details of the image that in many cases result to be hidden by the strongest sources.

Future studies will address a semiblind deconvolution approach [14, 15], in which Space-D could be used within an alternating minimization scheme [8] to deduce exact values for the roll angles α (that now are arbitrarily assumed to be uniformly distributed in each of the nine circles). Moreover, if combined with an existing software which infers the Fourier Transform of the emitting source (instead of the emission flux) [27, 29], images of the emitting particles could be reproduced.

REFERENCES

[1] J. Barzilai - J. M. Borwein, *Two point step size gradient methods*, IMA J. Numer. Anal., 8 (1988), 141-148.

[2] F. Benvenuto - R. Zanella - L. Zanni - M. Bertero, *Nonnegative least-squares image deblurring: improved gradient projection approaches*, Inverse Probl., **26** (2010), 025004.

[3] M. Bertero - P. Boccacci, *Introduction to inverse problems in imaging*, Institute of Physics Publishing-Bristol, 1998.

[4] M. Bertero - C. De Mol - E. R. Pike, *Linear inverse problems with discrete data: I - General formulation and singular system analysis*, Inverse Probl., **1** (1985), 300-330.

[5] D. Bertsekas, *Nonlinear programming*, Athena Scientific-Belmont, 1999.

[6] E. G. Birgin - J. M. Martinez - M. Raydan, *Inexact spectral projected gradient methods on convex sets*, IMA J. Numer. Anal., **23** (2003), 539-559.

[7] R. E. Blahut, *Theory of remote image formation*, Cambridge University Press-Cambridge, 2001.

[8] S. Bonettini, *Inexact block coordinate descent methods with application to the nonnegative matrix factorization*, IMA J. Numer. Anal., **37** (2011), 1431-1452.
[9] S. Bonettini - M. Prato, *Nonnegative image reconstruction from sparse Fourier data: a new deconvolution algorithm*, Inverse Probl., **26** (2010), 095001.
[10] S. Bonettini - M. Prato, *A novel gradient projection approach for Fourier-based image restoration*, AIP Conf. Proc., **1281** (2010), 527-530.
[11] S. Bonettini - R. Zanella - L. Zanni, *A scaled gradient projection method for constrained image deblurring*, Inverse Probl., **25** (2009), 015002.
[12] S. C. Bong - J. Lee - D. E. Gary - H. S. Yun, *Spatio-spectral maximum entropy method. I. Formulation and test*, Astrophys. J., **636** (2006), 1159-1165.
[13] R. N. Bracewell, *The Fourier transform and its applications*, McGraw-Hill-New York, 2000.
[14] J.-M. Conan - L. M. Mugnier - T. Fusco - V. Michau - G. Rousset, *Myopic deconvolution of adaptive optics images by use of object and point-spread function power spectra*, Appl. Opt., **37** (1998), 4614-4622.
[15] J. C. Christou - D. Bonnacini - N. Ageorges - F. Marchis, *Myopic deconvolution of adaptive optics images*, Messenger, **97** (1999), 14-22.
[16] B. R. Dennis - R. L. Pernak, *Hard X-ray flare source sizes measured with the Ramaty High Energy Solar Spectroscopic Imager*, Astrophys. J., **698** (2009), 2131-2143.
[17] A. Dutt - V. Rokhlin, *Fast Fourier Transforms for nonequispaced data*, SIAM J. Sci. Comput., **14** (1993), 1368-1393.
[18] B. Eicke, *Iteration methods for convexly constrained ill-posed problems in Hilbert space*, Numer. Func. Anal. Opt., **13** (1992), 413-429.
[19] H. W. Engl - M. Hanke - A. Neubauer, *Regularization of inverse problems*, Kluwer–Dordrecht, 1996.
[20] G. Frassoldati - G. Zanghirati - L. Zanni, *New adaptive stepsize selections in gradient methods*, J. Ind. Manage. Optim., **4** (2008), 299-312.
[21] S. F. Gull - G. J. Daniell, *Image reconstruction from incomplete and noisy data*, Nature, **272** (1978), 686-690.
[22] J. Hadamard, *Lectures on Cauchy's problem in linear partial differential equations*, Yale University Press–New Haven, 1923.
[23] G. J. Hurford - E. J. Schmahl - R. A. Schwartz - A. J. Conway - M. J. Aschwanden - A. Csillaghy - B. R. Dennis - C. Johns-Krull - S. Krucker - R. P. Lin - J. McTiernan - T. R. Metcalf - J. Sato - D. M. Smith, *The RHESSI imaging concept*, Solar Phys., **210** (2002), 61-86.
[24] S. Krucker - M. Battaglia - P. J. Cargill - L. Fletcher - H. S. Hudson - A. L. MacKinnon - S. Masuda - L. Sui - M. Tomczak - A. L. Veronig - L. Vlahos - S. M. White, *Hard X-ray emission from the solar corona*, Astron. Astrophys. Rev., **16** (2008), 155-208.
[25] R. P. Lin - B. R. Dennis - G. J. Hurford - D. M. Smith - A. Zehnder - P. R. Harvey - D. W. Curtis - D. Pankow - P. Turin - M. Bester - A. Csillaghy - M. Lewis - N. Madden - H. F. van Beek - M. Appleby - T. Raudorf - J. McTiernan - R. Ramaty - E. Schmahl - R. Schwartz - S. Krucker - R. Abiad - T. Quinn - P. Berg - M. Hashii - R. Sterling - R. Jackson - R. Pratt - R. D. Campbell - D. Malone - D. Landis - C. P. Barrington-Leigh - S. Slassi-Sennou - C. Cork - D. Clark - D. Amato - L. Orwig - R. Boyle - I. S. Banks - K. Shirey - A. K. Tolbert - D. Zarro - F. Snow - K. Thomsen - R. Henneck - A. Mchedlishvili - P. Ming - M. Fivian - J. Jordan - R. Wanner - J. Crubb - J. Preble - M. Matranga - A. Benz - H. Hudson - R. C. Canfield - G. D.

HOLMAN - C. CRANNELL - T. KOSUGI - A. G. EMSLIE - N. VILMER - J. C. BROWN - C. JOHNS-KRULL - M. ASCHWANDEN - T. METCALF - A. CONWAY, *The Reuven Ramaty High-Energy Solar Spectroscopic Imager (RHESSI)*, Solar Phys., **210** (2002), 3-32.

[26] A. M. MASSONE - A. G. EMSLIE - G. J. HURFORD - M. PRATO - E. P. KONTAR - M. PIANA, *Hard X-ray imaging of solar flares using interpolated visibilities*, Astrophys. J., **703** (2009), 2004-2016.

[27] M. PRATO, *Regularization methods for the solution of inverse problems in solar X-ray and imaging spectroscopy*, Arch. Comput. Methods Eng., **16** (2009), 109-160.

[28] M. PRATO - R. CAVICCHIOLI - L. ZANNI - P. BOCCACCI - M. BERTERO, *Efficient deconvolution methods for astronomical imaging: algorithms and IDL-GPU codes*, Astron. Astrophys., **539** (2012), A133.

[29] M. PRATO - M. PIANA - A. G. EMSLIE - G. H. HURFORD - E. P. KONTAR - A. M. MASSONE, *A regularized visibility-based approach to astronomical imaging spectroscopy*, SIAM J. Imag. Sci., **2** (2009), 910-930.

[30] T. SERAFINI - G. ZANGHIRATI - L. ZANNI, *Gradient projection methods for quadratic programs and applications in training support vector machines*, Optim. Methods Softw., **20** (2005), 353-378.

[31] A. N. TIKHONOV - A. V. GONCHARSKY - V. V. STEPANOV - A. G. YAGOLA, *Numerical methods for the solution of ill-posed problems*, Kluwer-Dordrecht, 1995.

[32] R. ZANELLA - P. BOCCACCI - L. ZANNI - M. BERTERO, *Efficient gradient projection methods for edge-preserving removal of Poisson noise*, Inverse Probl., **25** (2009), 045010.

[33] B. ZHOU - L. GAO - Y. H. DAI, *Gradient methods with adaptive step-sizes*, Comput. Optim. Appl., **35** (2006), 69-86.

Dipartimento di Scienze Fisiche, Informatiche e Matematiche
Università di Modena e Reggio Emilia, Via Campi 213/b, 41125 Modena, Italy
E-mail: marco.prato@unimore.it

Received November 14, 2012 and accepted April 27, 2013